



Thomas Jefferson University
Jefferson Digital Commons

Department of Biochemistry and Molecular Biology Faculty Papers Department of Biochemistry and Molecular Biology

10-6-2017

Complex interplay of kinetic factors governs the synergistic properties of HIV-1 entry inhibitors.

Koree W. Ahn


Thomas Jefferson University, koree.ahn@jefferson.edu

Michael J. Root

Thomas Jefferson University, michael.root@jefferson.edu

[Let us know how access to this document benefits you](#)

Follow this and additional works at: <https://jdc.jefferson.edu/bmpfp>

 Part of the [Medical Biochemistry Commons](#), and the [Medical Molecular Biology Commons](#)

Recommended Citation

Ahn, Koree W. and Root, Michael J., "Complex interplay of kinetic factors governs the synergistic properties of HIV-1 entry inhibitors." (2017). *Department of Biochemistry and Molecular Biology Faculty Papers*. Paper 127.

<https://jdc.jefferson.edu/bmpfp/127>

This Article is brought to you for free and open access by the Jefferson Digital Commons. The Jefferson Digital Commons is a service of Thomas Jefferson University's [Center for Teaching and Learning \(CTL\)](#). The Commons is a showcase for Jefferson books and journals, peer-reviewed scholarly publications, unique historical collections from the University archives, and teaching tools. The Jefferson Digital Commons allows researchers and interested readers anywhere in the world to learn about and keep up to date with Jefferson scholarship. This article has been accepted for inclusion in Department of Biochemistry and Molecular Biology Faculty Papers by an authorized administrator of the Jefferson Digital Commons. For more information, please contact: JeffersonDigitalCommons@jefferson.edu.



Complex interplay of kinetic factors governs the synergistic properties of HIV-1 entry inhibitors

Received for publication, April 17, 2017, and in revised form, July 9, 2017. Published, Papers in Press, July 10, 2017, DOI 10.1074/jbc.M117.791731

Koree W. Ahn and Michael J. Root¹

From the Department of Biochemistry and Molecular Biology, Sidney Kimmel Medical College, Thomas Jefferson University, Philadelphia, Pennsylvania 19107

Edited by Charles E. Samuel

The homotrimeric HIV-1 envelope glycoprotein (Env) undergoes receptor-triggered structural changes that mediate viral entry through membrane fusion. This process is inhibited by chemokine receptor antagonists (CoRAs) that block Env-receptor interactions and by fusion inhibitors (FIs) that disrupt Env conformational transitions. Synergy between CoRAs and FIs has been attributed to a CoRA-dependent decrease in the rate of viral membrane fusion that extends the lifetime of the intermediate state targeted by FIs. Here, we demonstrated that the magnitude of CoRA/FI synergy unexpectedly depends on FI-binding affinity and the stoichiometry of chemokine receptor binding to trimeric Env. For C-peptide FIs (clinically represented by enfuvirtide), synergy waned as binding strength decreased until inhibitor combinations behaved additively. Curiously, this affinity dependence on synergy was absent for 5-Helix-type FIs. We linked this complex behavior to the CoRA dependence of Env deactivation following FI binding. For both FI classes, reducing chemokine receptor levels on target cells or eliminating competent chemokine receptor-binding sites on Env trimers resulted in a loss of synergistic activity. These data imply that the stoichiometry required for CoRA/FI synergy exceeds that required for HIV-1 entry. Our analysis suggests two distinct roles for chemokine receptor binding, one to trigger formation of the FI-sensitive intermediate state and another to facilitate subsequent conformational transitions. Together, our results could explain the wide variety of previously reported activities for CoRA/FI combinations. These findings also have implications for the combined use of CoRAs and FIs in antiviral therapies and point to a multifaceted role for chemokine receptor binding in promoting HIV-1 entry.

The envelope glycoprotein (Env)² of human immunodeficiency virus-type 1 (HIV-1) is composed of gp120 and gp41

This work was supported by National Institutes of Health Grant R01 GM066682 (to M. J. R.). The authors declare that they have no conflicts of interest with the contents of this article. The content is solely the responsibility of the authors and does not necessarily represent the official views of the National Institutes of Health.

This article was selected as one of our Editors' Picks.

¹ To whom correspondence should be addressed: Dept. of Biochemistry and Molecular Biology, Thomas Jefferson University, 233 S. 10th St., Rm. 802, Philadelphia, PA 19107. Tel.: 215-503-4564; Fax: 215-923-2117; E-mail: michael.root@jefferson.edu.

² The abbreviations used are: Env, HIV-1 envelope glycoprotein; N-HR, N-terminal heptad repeat sequence of the gp41 ectodomain; C-HR, C-terminal heptad repeat sequence of the gp41 ectodomain; PHI, prehairpin interme-

diate; TOH, trimer-of-hairpins; CoRA, chemokine receptor antagonist; FI, fusion inhibitor; PBMC, peripheral blood mononuclear cell.

subunits arranged as a trimer of heterodimers in the viral membrane (1). It is formed through trimerization in the endoplasmic reticulum of precursor protein gp160, which is subsequently cleaved into a surface (gp120) and transmembrane (gp41) subunit that remain noncovalently associated. The three gp120 subunits form a canopy that cradles a trimeric gp41 core and locks the transmembrane protein in a metastable conformation (2–4). Trimerization is stabilized through gp120–gp120 interactions involving the V1/V2 and V3 variable loops at the apex of the complex and through a coiled coil formed by part of an N-terminal heptad repeat (N-HR) in the gp41 ectodomain (5–7).

Env undergoes receptor-triggered conformational changes to promote HIV-1 entry through membrane fusion (8–10). The gp120 subunits interact with cellular CD4, altering the Env apex to release constraints on the V3 loops. The released V3 loop and an additional newly formed gp120 element (bridging sheet) can now interact with a chemokine receptor, typically CCR5 or CXCR4 (collectively referred to as the coreceptor) (11–15). Receptor interactions also alter the gp120/gp41 interface and coordinate a complex series of structural changes in the transmembrane subunit (8, 9). First, each gp41 extends to insert its N-terminal fusion peptide segment into the target cell membrane. During this intermediate state (denoted the prehairpin intermediate or PHI), the N-HR coiled coil and an additional heptad repeat segment at the C terminus of the gp41 ectodomain (C-HR) become transiently exposed to the extracellular environment (16–20). Driven by a strong affinity for one another, the N-HR coiled coil associates with the three C-HR domains to form a compact trimer-of-hairpins (TOH) (21, 22). Collapse into the TOH juxtaposes the fusion peptides, transmembrane regions, and their associated membranes in a manner required for viral membrane fusion (10).

Molecules that block Env interactions with cellular receptors or disrupt Env conformational changes can effectively inhibit HIV-1 entry (23). Two classes of such molecules are currently used in the clinic. The first, denoted coreceptor antagonists (CoRAs), binds to the extracellular loops and transmembrane helices of CXCR4 or CCR5, blocking their interaction with the V3 loop of gp120 (24). The second, denoted fusion inhibitors (FIs), binds to the gp41 N-HR coiled coil or C-HR segments, blocking their ability to form the TOH (25–30). The clinically approved drugs maraviroc (CoRA) and enfuvirtide (FI, also denoted T20) are currently employed as second line therapy

diate; TOH, trimer-of-hairpins; CoRA, chemokine receptor antagonist; FI, fusion inhibitor; PBMC, peripheral blood mononuclear cell.

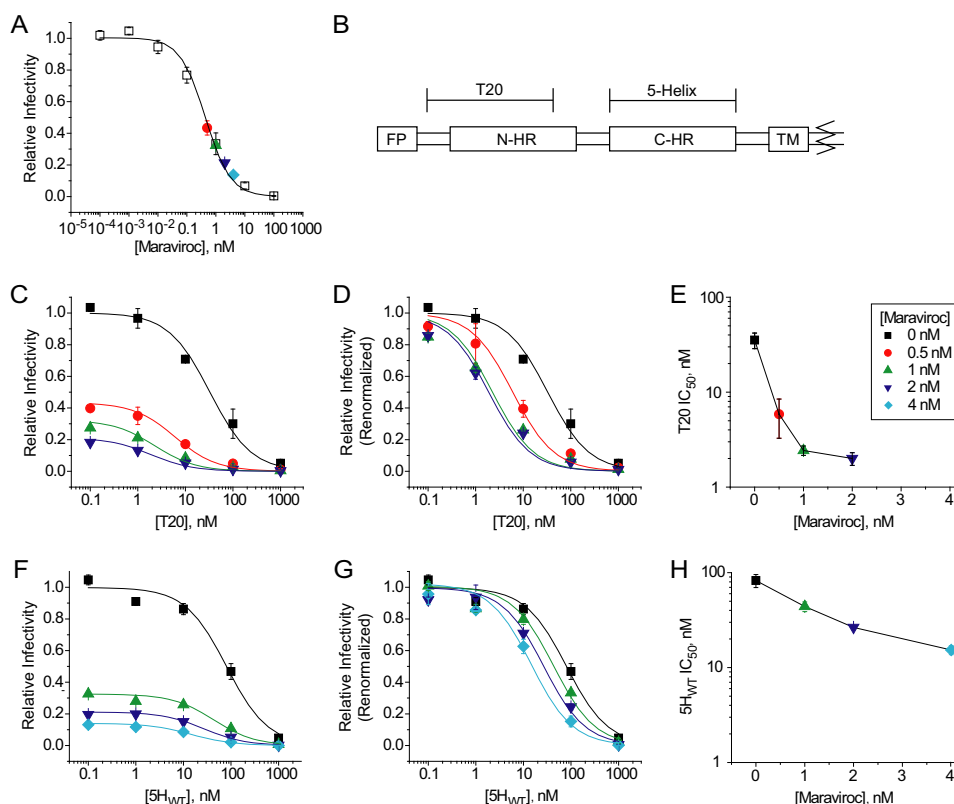


Figure 1. Combinatorial activities of CoRA maraviroc and FIs T20 and 5-Helix against Env_{JR-FL}. A, maraviroc titration of HIV-1 infection in the absence of FIs. Data have been normalized to the infection level in the absence of inhibitor. Data at maraviroc concentrations 0.5 (red), 1 (green), 2 (dark blue), and 4 nM (cyan) have been highlighted as these concentrations were used for combinatorial studies. The measured IC₅₀ value is 0.45 ± 0.15 nM. B, schematic of gp41 depicting the relative positions of the fusion peptide (FP), N-HR, C-HR, and transmembrane (TM) segments of the ectodomain. Binding sites for T20 and 5-Helix are designated. C, titration of T20 in the absence (black) and presence of maraviroc (colored as in A). Data have been normalized to the infection level in the absence of either entry inhibitor. D, T20 titrations shown in C renormalized to the level of infection in the absence of T20 and the presence of maraviroc (if any). E, plot of IC₅₀ for T20 inhibition as a function of maraviroc concentration. IC₅₀ values were determined from the titration curves shown in D. F–H, data for 5-Helix inhibition displayed as described in C–E. Data points and error bars represent the mean ± S.E. of three or more independent experiments. Titrations have been fit (solid lines) with a simple dose-response equation to extract IC₅₀ values (see Equation 1).

and used when traditional highly active antiretroviral therapy (HAART) becomes ineffective (31–34).

Based on their mechanisms of action, CoRAs and FIs should display synergistic activity when used in combination. Because the gp41 N-HR and C-HR are only transiently exposed during the PHI, FI potency depends on kinetics of inhibitor binding and Env dynamics (16, 17, 19, 35–39). An important determinant of FI activity is the lifetime of the PHI, a property that critically depends on Env interactions with chemokine receptors. Reducing either coreceptor levels on target cells or their binding affinity for gp120 decreases the rate of Env-mediated membrane fusion, prolonging the lifetime of the PHI (19, 35, 38–42). Because FIs have more time to bind gp41 during this prolonged PHI, their potency is enhanced. Theoretically, CoRAs should have the same functional effect as reducing coreceptor levels on target cells.

Surprisingly, studies of CoRA/FI combinations have produced inconsistent results. Although some reports have shown strong synergy between FIs and CoRAs (or coreceptor-binding proteins such as RANTES (regulated on activation normal T cell expressed and secreted) or monoclonal antibodies) (43–45), a number of studies have revealed only weak synergy or additivity between these two inhibitor classes (31, 45, 46). In one study exploring combinations of CoRA SCH-C and T20 on

activated peripheral blood mononuclear cells (PBMCs), three of six CCR5-tropic clinical HIV-1 isolates showed little or no synergy at all inhibitor concentrations, whereas the others showed strongly dose-dependent synergy (47). Here, we investigated the origins of this variability by exploring the inhibitory properties of different CoRA/FI combinations against different Env variants. Our findings revealed that the mechanism of synergy is more complex than originally postulated. We showed that the degree of CoRA/FI synergy strongly depends on FI-binding affinity and on coreceptor-Env binding stoichiometry. The results have implications for the effectiveness of clinical therapies involving CoRA/FI combinations and for the role of coreceptor binding in coordinating Env structural changes during HIV-1 entry.

Results

Measurement of synergy between FIs and CoRAs

There are a number of strategies to quantify the synergistic, additive, or antagonistic properties of inhibitor combinations (48–50). In this study, we focused specifically on the impact of CoRAs on the inhibitory potency of FIs. Our strategy is outlined in Fig. 1, A and C–E, on data obtained using inhibitors maraviroc and T20. HIV-1 pseudotyped with primary isolate Env_{JR-FL}

Complex synergy mechanisms of HIV-1 entry inhibitors

was utilized to infect U87-CD4-CCR5 target cells. The IC_{50} (IC_{50} indicates 50% inhibitory concentration) value for maraviroc in the absence of FI was first determined through careful titrations to be 0.45 nM (Fig. 1A). FI titrations were subsequently performed in the absence or presence of maraviroc at various concentrations (0.5, 1, and 2 nM, Fig. 1C). All titrations were fit to a simple dose–response relationship (Langmuir equation, see below) to extract IC_{50} values. To best appreciate the impact of maraviroc on FI potency, we renormalized each FI titration to the level of infection obtained in the absence of FI (Fig. 1D). The leftward shift of these renormalized curves in the presence of CoRA indicates an increase in T20 potency with increasing maraviroc concentrations. T20 IC_{50} values decreased from 35 to 2 nM as the maraviroc concentration was raised from 0 to 2 nM, reflecting a 17-fold improvement in FI potency (Fig. 1E).

The decrease in the FI IC_{50} value as CoRA concentration increases is a direct measure of synergistic activity. To appreciate this reasoning, assume that maraviroc and the FIs displayed additive activity. The probability of viral entry (P_{entry}) in the presence of a single inhibitor can be modeled as shown in Equation 1.

$$P_{\text{entry}} = \frac{1}{1 + \frac{[\text{inhibitor}]}{IC_{50}(\text{inhibitor})}} \quad (\text{Eq. 1})$$

For inhibitors that do not compete for the same site, additive combinatorial activity can be modeled as the product of individual entry probabilities as shown in Equation 2.

$$P_{\text{entry}} = \frac{1}{1 + \frac{[\text{CoRA}]}{IC_{50}(\text{CoRA})}} \cdot \frac{1}{1 + \frac{[\text{FI}]}{IC_{50}(\text{FI})}} \quad (\text{Eq. 2})$$

Under additive interactions, the presence of CoRA will only impact the scale of FI titrations but not their IC_{50} values. Hence, renormalized FI titrations (e.g. Fig. 1D) should overlap, and the FI IC_{50} versus CoRA concentration plot (e.g. Fig. 1E) should be horizontal. However, if the two inhibitors interact synergistically, then the IC_{50} values of the normalized FI titrations will be less in the presence than in the absence of CoRA (as observed). Conversely, if the two inhibitors interacted antagonistically, then the IC_{50} values of the normalized FI titrations will be greater in the presence than in the absence of CoRA. The analysis employed here shares a common logic with the calculation of combination indices developed by Chou and Talalay and routinely used to quantify drug combinatorial properties (48). Expanding the product in Equation 2 yields Equation 3.

$$P_{\text{entry}} = \frac{1}{1 + \frac{[\text{CoRA}]}{IC_{50}(\text{CoRA})} + \frac{[\text{FI}]}{IC_{50}(\text{FI})} + \frac{[\text{CoRA}] \cdot [\text{FI}]}{IC_{50}(\text{CoRA}) \cdot IC_{50}(\text{FI})}} \quad (\text{Eq. 3})$$

The last three terms of the denominator are equivalent to the value of the combination index at 50% inhibition for mutually nonexclusive inhibitors.

FI T20 is an example of a C-peptide, so named because they are derived from the gp41 C-HR segment. C-peptides block entry by binding to the gp41 N-HR coiled coil exposed in the PHI (17, 20, 27, 51). We next asked whether FIs that work in a complementary manner by targeting gp41 C-HR region would show similar synergistic activity with CoRAs. We used 5-Helix ($5H_{\text{WT}}$), an engineered protein containing three N-HR segments and two C-HR segments alternately connected through short Gly/Ser linkers (28). When properly folded, $5H_{\text{WT}}$ exposes a single high-affinity site that binds the gp41 C-HR region during the PHI. Like T20, $5H_{\text{WT}}$ showed significantly improved inhibitory activity in the presence of maraviroc (Fig. 1, *F–H*). However, we did observe considerable differences between the two FIs. First, the magnitude of synergy for $5H_{\text{WT}}$ was substantially less, with IC_{50} falling from 83 to 15 nM (a 5.5-fold change) when the maraviroc concentration was raised from 0 to 4 nM. Second, T20 activity was much more sensitive to maraviroc concentration than $5H_{\text{WT}}$ activity; the impact on T20 potency appeared to saturate at ~ 1 nM maraviroc, whereas the impact on $5H_{\text{WT}}$ potency did not saturate in the studied maraviroc concentration range. The differences likely reflect an asymmetry in exposure of the gp41 N-HR and C-HR regions and/or differences in the determinants of potency for FIs that target these sites (36, 38).

Dependence of C-peptide FI/CoRA synergy on C-peptide-binding affinity

As a potential source of variability in reported inhibitor combination studies, we asked whether the properties of CoRA/FI synergy were altered in the presence of Env mutations that disrupt FI-binding affinity. In these experiments, we used HIV-1 pseudotyped with CXCR4-tropic Env_{HXB2}, U87-CD4-CXCR4 target cells, and CoRA AMD3100. The FI was C37, a well-characterized C-peptide with a binding site that overlaps that for T20 (38, 52). As with maraviroc/T20 combinations in Fig. 1, C37 IC_{50} decreased from 2.8 to 0.37 nM (7.4-fold) as AMD3100 concentration was increased from 0 to 100 nM (Fig. 2C). We next analyzed a mutant Env variant containing the V549E substitution known to disrupt C37-binding affinity by 5000-fold and reduce C37 inhibitory potency by 100-fold (Table 1) (38, 53). The mutation did not alter the potency of AMD3100 ($IC_{50} \sim 26$ nM), implying that the V549E substitution did not affect Env utilization of the coreceptor (Fig. 2B). By contrast, the mutation ablated synergistic activity between AMD3100 and C37 observed for wild-type Env (Fig. 2, C and D); C37 IC_{50} values for the V549E Env variant in the presence of 0 and 100 nM AMD3100 were essentially identical (~ 200 nM). The data suggested that AMD3100/C37 combinatorial activity was influenced by FI-binding affinity.

To confirm the importance of binding affinity on the magnitude of CoRA/FI synergy, we studied the combinatorial activities of AMD3100 and mutant C37 variants with altered binding affinity. We first explored the inhibitory properties of two mutant C37 variants with lower binding affinities, C37_{W628A} (50-fold lower affinity) and C37_{N656D} (4000-fold lower) (38). Consistent with their reduced binding affinities, the mutant C37 variants displayed lower potency against wild-type Env (Table 1 and Fig. 3A). Moreover, they also showed significantly

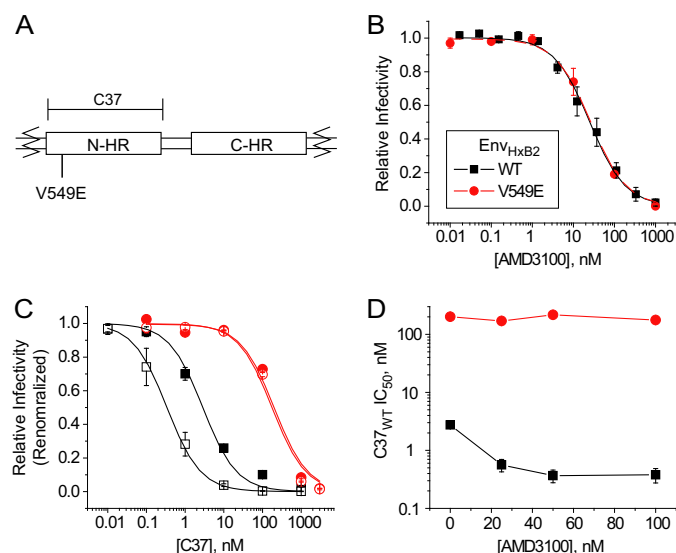


Figure 2. Combinatorial activities of CoRA AMD3100 and FI C37 against wild-type Env_{HXB2} and the V549E mutant variant. *A*, schematic of the gp41 ectodomain depicting the binding site for C37 and the relative position of the V549E substitution. *B*, AMD3100 titrations of wild-type (black) and V549E mutant (red) Env. The measured IC₅₀ values were 26 ± 4.1 and 27 ± 6.4 nM, respectively. *C*, C37 titration of wild-type (black) and V549E mutant (red) Env in the absence (filled symbols) and presence (open symbols) of 100 nM AMD3100. Data have been renormalized to the level of infection in the absence of C37 and the presence of AMD3100 (if any). *D*, IC₅₀ values for wild-type and V549E mutant Env as a function of AMD3100 concentration. Note that the following data have been repeated in subsequent figures for comparative purposes: AMD3100 titration of wild-type Env_{HXB2} (black squares in *B*, repeated in Figs. 4*B*, 5*B*, and 7*C*); C37 titration of wild-type Env_{HXB2} (black squares in *C*, repeated in Fig. 7*D*); C37 IC₅₀ values for wild-type Env_{HXB2} as a function of AMD3100 concentration (black squares in *D*, repeated in Fig. 3*A* as green squares and in Fig. 7*E* as black squares); C37 IC₅₀ values for the V549E Env_{HXB2} mutant variant as a function of AMD3100 concentration (red circles in *D*, repeated in Fig. 3*B* as green squares).

reduced synergistic activities in combination with AMD3100. For C37_{W628A}, FI IC₅₀ improved only 2.5-fold in the presence of high concentrations of AMD3100 (compared with 7.4-fold for wild-type C37). For C37_{N656D}, the presence of AMD3100 did not alter FI IC₅₀ even at high CoRA concentrations.

Combined, the data suggested that reducing C-peptide-binding affinity decreased the magnitude of FI-CoRA synergy. We next asked whether the converse was true. Did increasing C-peptide affinity result in greater synergistic activity of this drug combination? We employed two additional C37 variants with enhanced affinity, C37-KYI (16-fold higher) and di-C37 (greater than 100-fold higher) (38). Against wild-type Env, the enhanced binding affinity did not translate to higher potency compared with C37, consistent with a kinetic restriction on their inhibition (Table 1 and Fig. 3*A*) (see below and Ref. 38). Moreover, C37-KYI and di-C37 displayed synergy with AMD3100 that mimicked AMD3100/C37 synergy against wild-type Env in terms of magnitude and CoRA dependence. By contrast, the enhancement of FI affinity significantly impacted inhibition of the V549E Env variant (Table 1 and Fig. 3*B*). On the one hand, C37-KYI potency was improved almost 20-fold, but it still showed the same additive activity as C37 in combination with AMD3100. On the other hand, di-C37 potency was improved ~100-fold and showed substantial synergy in combination with the CoRA. In fact, the potency of di-C37 and the magnitude and CoRA dependence of AMD3100/di-C37 syn-

Table 1
Inhibitory and binding properties of C37 and 5-Helix FIs

IC₅₀ (upper left) and K_D (upper right) values are given in nanomolar concentrations; k_{on} values (middle right) are in units of $M^{-1} s^{-1}$; and k_{off} values (lower right) are in units of s^{-1} . K_D and k_{on} values were measured using an *in vitro* binding assay employing the designated C37 and 5-Helix variants (19, 38); these parameters were used to calculate k_{off} values: $k_{off} = K_D \cdot k_{on}$. IC50 values were measured for inhibition of Env_{HXB2}-mediated HIV-1 infection of U87.CD4.CXCR4 cells performed in this study. Green boxes indicate FI/Env pairs with kinetically restricted potency ($k_{off} < 0.2 \cdot k_s$, see text). Red boxes indicate FI/Env pairs with affinity-dependent potency ($k_{off} > 5 \cdot k_s$). Yellow boxes indicate FI/Env pairs with potency dependent on both kinetic and equilibrium factors (k_{off} values within 2-fold of k_s). Env_{HXB2} k_s values, estimated from a previous study (38), are $4.9 \times 10^{-4} s^{-1}$ for C37 inhibitors and 0.11 s^{-1} for 5-Helix inhibitors. *, nd means not determined.

		Env _{HXB2} Variant					
		N-HR Substitutions			C-HR Substitutions		
Inhibitor	WT	V549E	L565Q	N637K/ T639I	N656S	N656D	
C37	2.8 0.00065 3.0×10^7 2.0×10^{-5}	201 8.1 0.63×10^7 0.051	nd 0.025 1.5×10^7 3.8×10^{-4}				
C37 _{W628A}	14 0.033 1.5×10^7 5.0×10^{-4}						
C37 _{N656D}	105 2.5 2.6×10^7 0.065						
C37-KYI	2.3 0.00004 2.4×10^7 9.6×10^{-7}	5.3 0.49 0.55×10^7 0.0027					
di-C37	2.3 <0.00001 nd nd	2.2 nd nd nd	0.2 nd nd nd	4.3 nd nd nd			
5H _{WT}	56 0.00065 3.0×10^7 2.0×10^{-5}		3.9 0.00065 3.0×10^7 2.0×10^{-5}	400 0.00004 2.4×10^7 9.6×10^{-7}	52 0.020 3.1×10^7 6.2×10^{-4}	50 3.0 2.3×10^7 0.069	
5H _{ΔVA}	107 8.3 1.2×10^7 0.099				1000 > 1.0×10^7 >5.3	530 > 1.0×10^7 >36	>3000 > 1.0×10^7 >36

IC50
 k_D
 k_{on}
 k_{off}

ergy were nearly identical for the wild-type and the V549E Env variants. Thus, CoRA/C-peptide synergy was restored for an Env variant with an affinity-disrupting mutation by sufficiently dialing up the binding strength of the FI. The data implied that CoRA/C-peptide synergy required a high-affinity interaction between the C-peptide and gp41.

Modeling the impact of CoRA on C-peptide inhibition

Our data indicated that the antiviral activity of CoRA/C-peptide combinations depended on the affinity of C-peptide interactions. We previously showed that the factors determining C-peptide potency differed for high and low-affinity inhibitors. The discrepancy was best appreciated by modeling intermediate state inhibition as shown in Fig. 3*C*. Here, N, I, and F represent the native, intermediate, and fusogenic conformations. Fusion inhibitors (X) bind the intermediate state (IX) and promote transition into an irreversibly deactivated state (D). Rate constants k_f and k_s describe the $N \rightarrow F$ and $IX \rightarrow D$ transitions, respectively, whereas k_{on} and k_{off} denote inhibitor association and dissociation from gp41. Based on this model, Equation 4 for fusion inhibitor IC₅₀ was derived (19).

$$IC_{50} = \frac{k_f}{k_{on}} \left(1 + \frac{k_{off}}{k_s} \right) = \frac{k_f}{k_{on}} + \frac{k_f}{k_s} K_D \quad (\text{Eq. 4})$$

For high-affinity and slowly dissociating FIs ($k_{off} \ll k_s$), inhibitor binding almost always leads to deactivation. In this case, inhibitory potency is determined primarily by how fast the

Complex synergy mechanisms of HIV-1 entry inhibitors

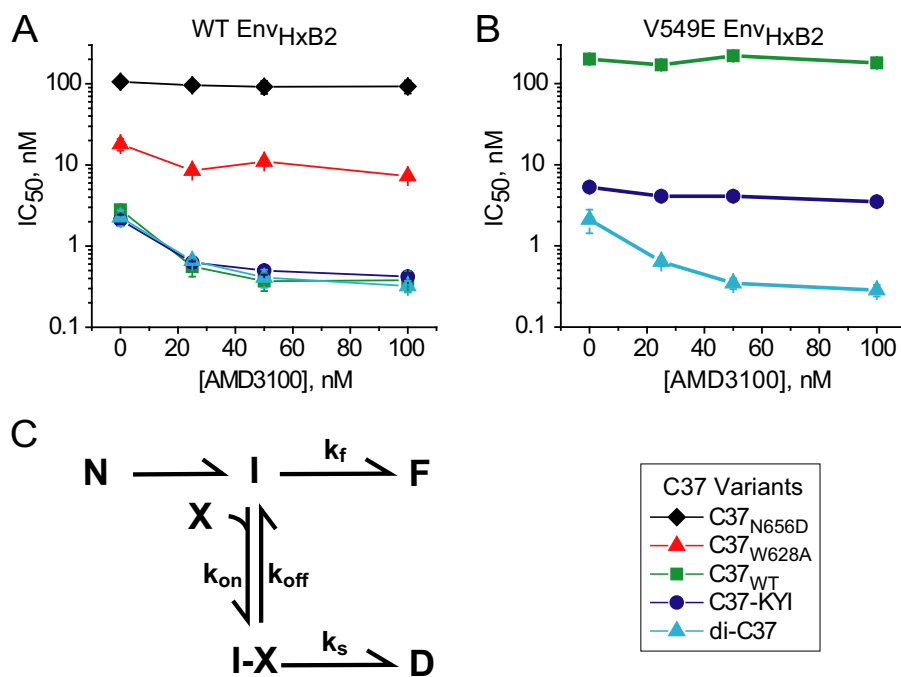


Figure 3. Dependence of AMD3100/C37 synergy on C37-binding affinity. A and B, FI IC₅₀ values for wild-type Env_{HXB2} (A) and V549E mutant Env (B) are plotted as a function of AMD3100 concentration. In order of increasing binding affinity, the C37 variants were C37_{N656D} (black), C37_{W628A} (red), C37 (wild-type, green), C37-KYI (blue), and di-C37 (cyan). C, schematic depiction of intermediate-state inhibition by C37 and other FIs. States and rate constants are defined in the text.

inhibitor can associate during the lifetime of the intermediate state: $IC_{50} \approx k_f/k_{on}$. This kinetic dependence explains why C37, C37-KYI, and di-C37 displayed the same potency against wild-type Env despite having widely varying binding affinities (Fig. 3A). In the proposed mechanism of synergy, CoRAs reduce the level of coreceptors capable of interacting with Env, thereby prolonging the intermediate state and increasing the chance of FI binding gp41. Quantitatively, this proposed effect describes a decrease in rate constant k_f which, in turn, results in a lower IC₅₀ value for high-affinity C-peptides.

For low-affinity, rapidly dissociating FIs ($k_{off} \gg k_s$), inhibitor association is most often followed by multiple cycles of dissociation and re-association before Env transitions into the fusogenic (F) or deactivated (D) state. Therefore, inhibitory potency depends upon binding affinity and the relative difference between the rates to states F and D: $IC_{50} \approx (k_f/k_s)K_D$. The dependence of potency on binding affinity explains the difference in IC₅₀ values for C37, C37-KYI, and di-C37 against the V549E Env variant (Fig. 3B). Our previous work has suggested that the rates k_f and k_s for C-peptides share the same dependence on cellular coreceptor levels (38).³ Thus, adding CoRA should induce the same fold-reduction in k_f and k_s , leaving their ratio unaltered and the IC₅₀ values for the low-affinity, rapidly dissociating C-peptides unchanged. Hence, we propose that the sim-

ilar dependence of the $I \rightarrow F$ and $Ix \rightarrow D$ transitions on cellular coreceptor levels leads to additive activity for combinations of CoRAs and low-affinity C-peptides.

Preservation of CoRA/5-Helix synergy under low-affinity 5-Helix interactions

Although both C-peptides and 5-Helix target gp41 during the PHI, our previous work showed that these two inhibitor classes induced Env deactivation through different mechanisms (38). Notably, the deactivation rate constant k_s for 5-Helix inhibition did not depend on cellular coreceptor levels. Therefore, we predicted that CoRA/5-Helix synergy should be largely independent of 5-Helix-binding affinity. We tested this prediction using Env_{HXB2} variants with C-HR mutations N656S and N656D, which reduced 5-Helix-binding affinity 30- and 5000-fold, respectively (Fig. 4A and Table 1) (38). All three Env variants showed the same sensitivity to AMD3100, indicating the C-HR substitutions did not impact CXCR4 utilization of Env_{HXB2} (Fig. 4B). We first used the wild-type version of 5-Helix (5H_{WT}), an extremely high-affinity fusion inhibitor with kinetically restricted potency ($IC_{50} \approx k_f/k_{on}$) against the wild-type and N656S Env variants and near kinetically restricted potency against the N656D Env variant (Table 1 and Fig. 4, C and E). As expected, the potency of 5H_{WT} was not altered by affinity-disrupting mutations in the C-HR region. Moreover, IC₅₀ values for 5H_{WT} decreased upon addition of AMD3100, consistent with a CoRA-dependent increase in the temporal exposure of the gp41 C-HR region (Fig. 4E).

Next, we used a mutant variant of 5-Helix (5H_{LAVA}) containing the L556A/V570A dual substitution that reduces the inhibitor-binding affinity 13,000-fold (19). 5H_{LAVA} binds relatively weakly to wild-type Env and even more poorly to the N656S and

³ It is not known why rate constant k_s for C-peptide inhibitors depends upon chemokine receptor levels on target cells. We have previously speculated (38) that the $Ix \rightarrow D$ transition follows the same conformational change as the $I \rightarrow F$ transition, except that the attached C-peptide prevents proper formation of the TOH, leading to irreversible misfolding of the gp41 ectodomain. This hypothesis predicts that k_s and k_f for C-peptide inhibitors would share the same dependence on target cell chemokine receptor levels, as is observed.

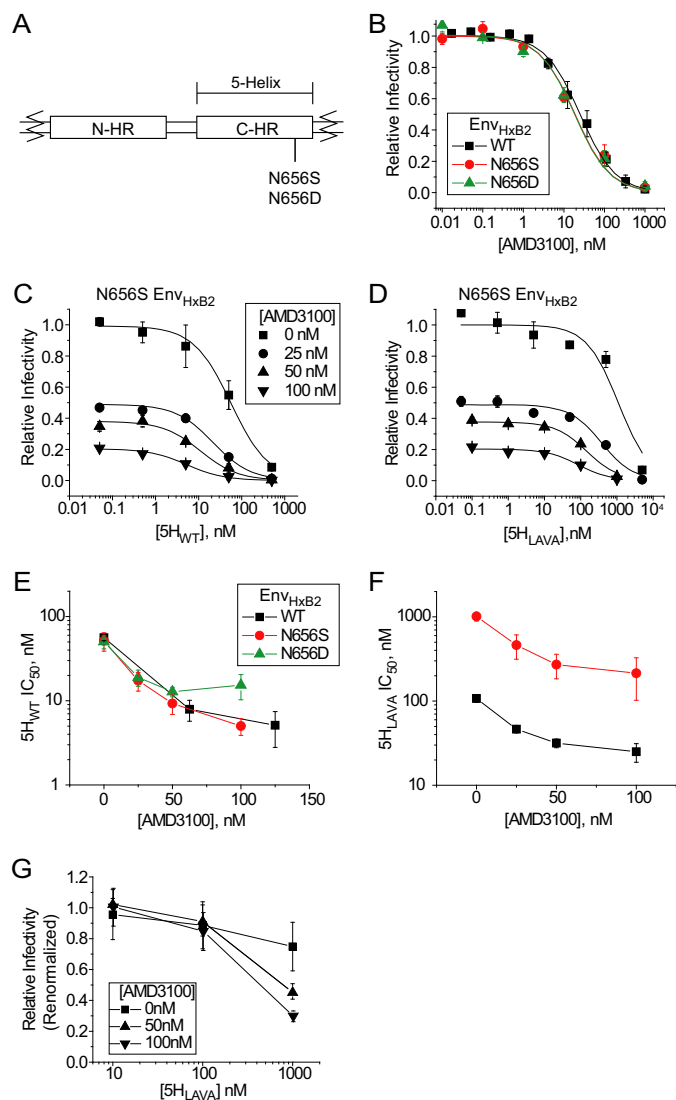


Figure 4. Maintenance of AMD3100/5-Helix synergy across a wide range of 5-Helix binding affinities. *A*, schematic of the gp41 ectodomain depicting the 5-Helix-binding site and relative position of the N656S and N656D substitutions. *B*, AMD3100 titrations of wild-type (black), N656S (red), and N656D (green) Env_{HXB2} variants. The measured IC₅₀ values were 26 ± 4.1, 19 ± 2.9, and 21 ± 5.5 nM, respectively. *C* and *D*, 5H_{WT} (*C*) and 5H_{LAVA} (*D*) titrations of the N656S Env variant in the absence (square) and presence of AMD3100 at 25 (circle), 50 (up triangle), and 100 nM (down triangle). Data have been normalized to the infectivity level in the absence of either inhibitor. *E* and *F*, IC₅₀ values for 5H_{WT} (*E*) and 5H_{LAVA} (*F*) as a function of AMD3100 concentration for wild-type (black), N656S (red), and N656D (green) Env. *G*, relative infectivity levels of N656D mutant Env in the absence (square) or presence of AMD3100 at 50 (up triangle) or 100 nM (down triangle) in the presence of the indicated concentrations of 5H_{LAVA}. Data have been normalized to the level of infectivity in the presence of AMD3100 and absence of 5H_{LAVA}. Note that the following data have been repeated in subsequent figures for comparative purposes: 5H_{WT} IC₅₀ values for wild-type Env_{HXB2} as a function of AMD3100 concentration (black squares in *E*, repeated in Figs. 5C and 7F).

N656D Env variants (Table 1). Importantly, the rate of 5H_{LAVA} dissociation from the mutant Env variants substantially exceeds the estimated rate of 5-Helix-induced gp41 deactivation ($k_{off} \gg k_s$, see Table 1). As expected for such a low-affinity FI, 5H_{LAVA} potency depended on its binding affinity ($IC_{50} \approx (k_f/k_s)K_D$, see Table 1). The IC₅₀ value was lowest against wild-type Env (110 nM), higher against the intermediate-affinity variant N656S Env (1000 nM), and highest against the most affinity-

disrupted variant N656D Env (>3000 nM). Despite interacting with low affinity, 5H_{LAVA} showed synergistic activity against all three Env variants. Against the wild-type and N656S Env variants, the magnitude and CoRA dependence of the AMD3100/5H_{LAVA} synergy closely mimicked those for AMD3100/5H_{WT} synergy (compare Fig. 4, *E* and *F*). The low potency of 5H_{LAVA} against the N656D Env variant precluded accurate determination of IC₅₀ values for a similar analysis. However, N656D Env was substantially more sensitive to 1000 nM 5H_{LAVA} in the presence of AMD3100 (50 and 100 nM) than in its absence (Fig. 4G). Thus, the synergy between AMD3100 and 5-Helix was not significantly influenced by 5-Helix-binding affinity, even when the rate of inhibitor dissociation exceeded the rate of gp41 deactivation. These results were consistent with the 5-Helix-induced deactivation rate constant k_s being independent of coreceptor levels on target cells.

Impact of k_f -altering gp41 mutations on CoRA/FI synergy

Certain gp41 mutations can influence the lifetime of the intermediate state without incurring a substantial disruption to FI-binding affinity (Fig. 5) (54, 55). The substitution L565Q in the N-HR elicits a decrease in fusion rate that is manifested by a 10-fold increase in sensitivity to kinetically restricted FI 5H_{WT} (Table 1). By contrast, the dual substitution N637K/T639I in the C-HR enhances fusion rate, resulting in a 10-fold decrease in 5H_{WT} sensitivity (Table 1). We questioned whether the effects of these gp41 mutations were mediated, in part, through altered coreceptor interactions and, if so, how that would impact CoRA/FI synergy. The IC₅₀ values for AMD3100 against L565Q Env and N637K/T639I Env were 63 and 17 nM, respectively, not substantially different from the 26 nM IC₅₀ value for wild-type Env (Fig. 5B). The data suggested that the substitutions minimally impacted CXCR4 utilization. The two mutant Env variants showed AMD3100/5H_{WT} synergy of comparable magnitude and CoRA dependence as that for wild-type Env (Fig. 5C). Similar results were observed for synergy between AMD3100 and the kinetically restricted FIs di-C37 and PIE12 trimer⁴ (56) that target the gp41 N-HR region (Fig. 5, *D* and *E*). Thus, our data suggested that these gp41 mutations altered an intrinsic rate of gp41 folding that can be further modified extrinsically through coreceptor binding.

Dissecting the dependence of FI/CoRA synergy on coreceptor binding

Close inspection of our synergy data revealed a tendency for FI IC₅₀ values to level off at high CoRA concentrations. The result suggested a limit to the degree that rate constant k_f could be reduced by lowering the levels of available coreceptor on target cells. Based on this observation, we predicted that the magnitude of CoRA/FI synergy would be smaller on target cells expressing lower levels of coreceptor. To test this prediction, we employed HeLa-derived JC.53 and JC.10 target cells that

⁴ PIE12 is a D-amino acid peptide selected by mirror-image phage display that binds a hydrophobic pocket at the C terminus of the N-HR coiled coil (56). In the PIE12 trimer, three PIE12 peptides are cross-linked using polyethylene glycol linkers to create a molecule capable of multivalent binding to the gp41 N-HR region exposed during the PHI.

Complex synergy mechanisms of HIV-1 entry inhibitors

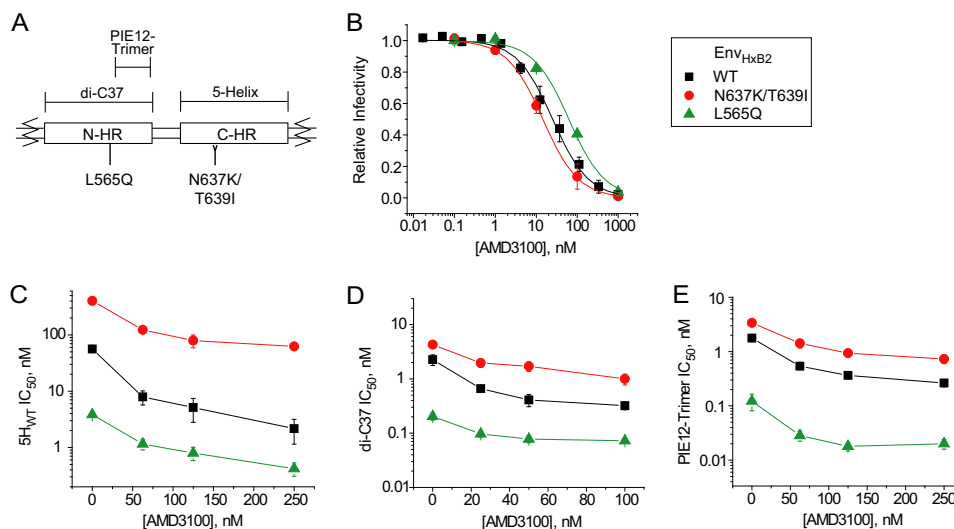


Figure 5. Impact of rate-altering gp41 mutations on CoRA/FI synergy. A, schematic of the gp41 ectodomain depicting the di-C37-, PIE12 trimer-, and 5-Helix-binding sites and the relative positions of the L565Q and N637K/T639I substitutions. The three inhibitors bind with extremely high affinity and have kinetically restricted inhibitory potencies. The L565Q substitution minimally disrupts on C37-binding affinity but significantly prolongs the PHI lifetime. The N637K/T639I substitution actually increases 5-Helix-binding affinity and shortens N-HR exposure modestly and C-HR exposure significantly. B, AMD3100 titration of wild-type (black), L565Q (green), and N637K/T639I (red) Env_{HXB2} variants. The measured IC₅₀ values were 26 ± 4.1, 63 ± 1.2, and 17 ± 6 nM, respectively. C–E, IC₅₀ values for 5H_{WT} (C), di-C37 (D), and PIE12 trimer (E) as a function of AMD3100 concentration for the three Env variants.

have similar levels of CD4 (4×10^5 per cell) but different levels of CCR5 (1.3×10^5 and 2.0×10^3 per cell, respectively) (57). The IC₅₀ value of CCR5 antagonist TAK-779 against HIV-1 pseudotyped with Env_{BaL} was lower on target cells expressing lower CCR5 levels (JC.10), consistent with previous conclusions that CoRAs competitively block chemokine receptor interactions with Env (Fig. 6A) (35, 39). Furthermore, the IC₅₀ value for kinetically restricted FI C37 was significantly lower on JC.10 cells compared with JC.53 cells, as expected for reduced CCR5 levels leading to a decreased rate constant k_f (Fig. 6B) (38). As predicted, CoRA/FI synergy differed between the two cell lines. For cells with high CCR5 levels (JC.53), FI IC₅₀ values decreased significantly (3–5-fold) in the presence of CoRA (Fig. 6, C and E). By contrast, for target cells with low levels of CCR5 (JC.10), FI IC₅₀ values showed minimal dependence (less than 2-fold) on CoRA concentrations (Fig. 6, D and E). This difference between cell lines was not dependent on FI target site (N-HR for C37 and C-HR for 5H_{WT}) and was observed for both laboratory-adapted (BaL, H5) and primary isolate (JRFL) Env strains (Fig. 6, E–H). Thus, FI/CoRA synergy appeared to require a sufficient level of chemokine receptors on target cells, below which inhibitor combinations behaved in an additive manner.

One explanation for these observations is that the coreceptor binding stoichiometry required for HIV-1 entry is less than the stoichiometry required to observe CoRA/FI synergy. To test this conjecture, we investigated the properties of Env trimers that contained less than three coreceptor-binding sites. We generated HIV-1 from cells coexpressing wild-type Env_{HXB2} (denoted H4) and a variant Env_{HXB2} with a V3-loop from the CCR5-tropic Env_{SF162} (denoted H5) (58). The V3-loop swap rendered H5 Env unable to mediate efficient viral entry on CXCR4⁺ target cells but capable of mediating robust fusion on CCR5⁺ cells. Coexpression of the two Env variants resulted in four trimeric species, (H4)₃, (H4)₂(H5), (H4)(H5)₂, and (H5)₃,

with the heterotrimers having a mixture of competent CXCR4- and CCR5-binding sites (Fig. 7A). To specifically focus on heterotrimer activity, H4/H5 expression was biased 1:19, and the resulting HIV-1 sample was applied to CXCR4⁺ cells (Fig. 7B). With this expression ratio, the predominant trimeric species, homotrimer (H5)₃, lacked a CXCR4-binding site and was not fusogenic. The other homotrimer, (H4)₃, was fusogenic but formed only a minuscule fraction of total Env trimers. The infectivity of this viral sample far exceeded the level predicted if only homotrimeric (H4)₃ contributed to membrane fusion (Fig. 7B). The result suggested that the heterotrimeric Envs containing either one or two CXCR4-binding sites were the predominant fusogenic species in this viral population.

HIV-1 pseudotyped with H4/H5 = 1:19 displayed significantly higher sensitivity to both AMD3100 and C37 compared HIV-1 pseudotyped with (H4)₃ homotrimers alone (Fig. 7, C and D). The results confirmed that Env heterotrimers contributed the majority of fusogenic activity in these mixed trimer viral samples. The enhanced sensitivity to AMD3100 likely reflected an increased requirement for CXCR4 on target cells to compensate for a reduced number of coreceptor-binding sites on fusogenic Env heterotrimers. The enhanced sensitivity to C37 probably resulted from slower fusion kinetics due to reduced coreceptor binding (similar to the impact of decreasing coreceptor levels on target cells). Notably, C37 IC₅₀ for HIV-1 pseudotyped with H4/H5 = 1:19 showed no dependence on AMD3100 concentration (Fig. 7E). Likewise, 5H_{WT} IC₅₀ against this viral population was minimally perturbed in the presence of AMD3100 (Fig. 7F). The results were in sharp contrast to the CoRA/FI synergy seen for HIV-1 pseudotyped with (H4)₃ homotrimers.

We repeated these experiments biasing H4/H5 expression 19:1 and using CCR5⁺ target cells (Fig. 8A). Again, the infectivity of viral samples containing mixed Env trimers exceeded that predicted if only (H5)₃ homotrimers contributed to viral entry

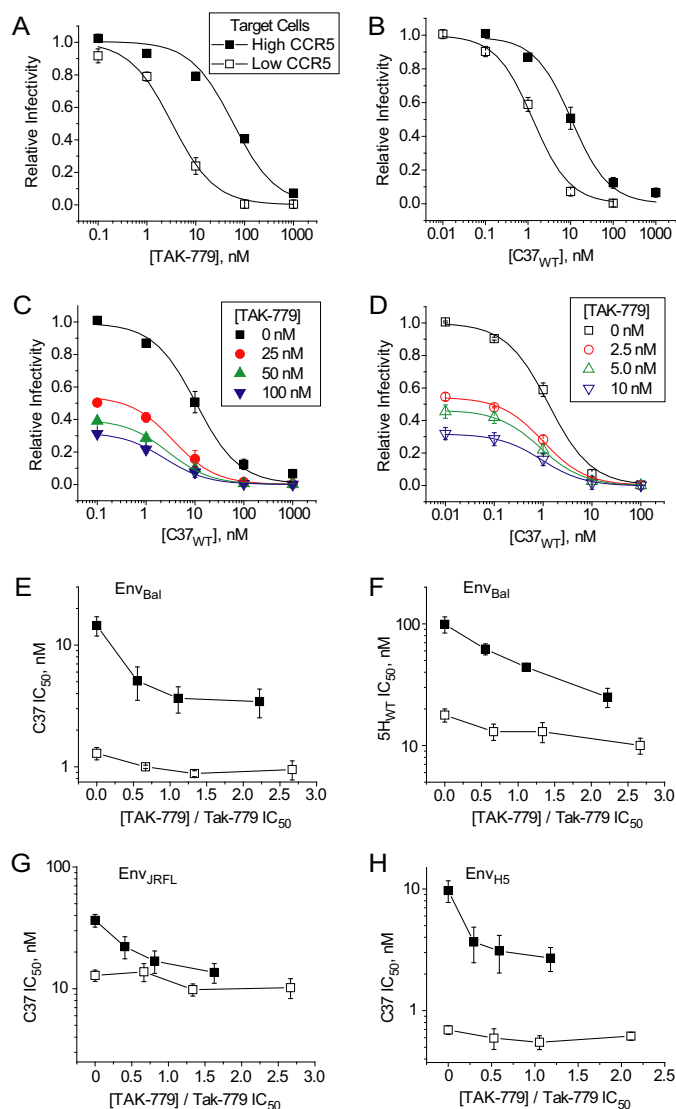


Figure 6. Impact of target cell chemokine receptor levels on CoRA/FI synergy. *A*, titration of CoRA TAK-779 against Env_{Bal}-mediated HIV-1 entry into JC.53 (high CCR5, filled squares) and JC.10 (low CCR5, open squares) target cells. The measured IC₅₀ values were 59 ± 3.4 and 3.3 ± 0.31 nM, respectively. *B*, C37 titration of Env_{Bal} on the two cell lines. The measured IC₅₀ values were 15 ± 2.6 and 1.3 ± 0.15 nM, respectively. *C*, C37 titrations of Env_{Bal} on JC.53 target cells (high CCR5) performed in the absence (black) and presence of 25 (red), 50 (green), and 100 nM (blue) TAK-779. *D*, C37 titrations of Env_{Bal} on JC.10 target cells (low CCR5) performed in the absence (black) and presence of 2.5 (red), 5 (green), and 10 nM (blue) TAK-779. *E* and *F*, IC₅₀ values for C37 (*E*) and 5H_{WT} (*F*) as a function of TAK-779 concentration for Env_{Bal} on JC.53 (high CCR5, filled squares) and JC.10 (low CCR5, open squares). *G* and *H*, C37 IC₅₀ values as a function of TAK-779 concentration for Env_{JRFL} (*G*) and Env_{H5} (*H*) on the two cell lines.

(Fig. 8B). Although expression of mixed trimers did not impact TAK-779 sensitivity, HIV-1 containing heterotrimers was much more sensitive to FI than HIV-1 expressing only (H5)₃ homotrimers (Fig. 8, C and D). As before, the CoRA/FI synergy observed for (H5)₃ homotrimers was largely absent when heterotrimers were the predominant fusogenic Env species (Fig. 8, E and F). Thus, regardless of which chemokine receptor was used for entry, reducing the number of coreceptor-binding sites on the Env trimer appeared to ablate the CoRA/FI synergy. The data supported our conjecture that CoRA/FI synergy required

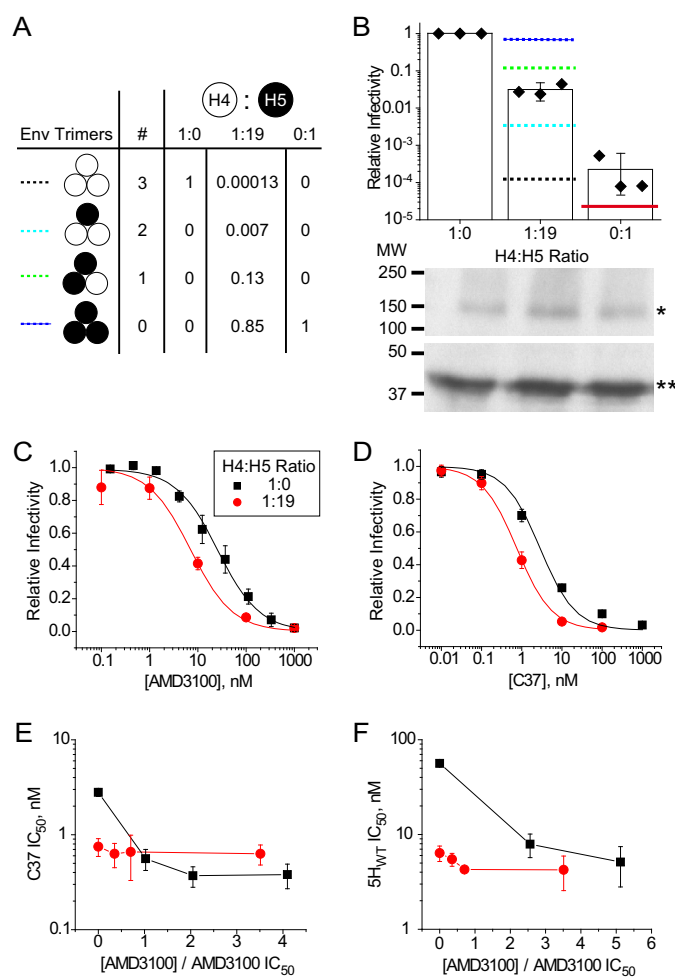


Figure 7. Impact of modifying the number of CXCR4-binding sites per Env_{HXB2} trimer on CoRA/FI synergy. *A*, mixed trimer population resulting from the coexpression of Env variants H4 (HXB2) and H5 in virus-producing cells. Each of the four possible trimeric species has a different number of competent CXCR4-binding sites (#). The fraction of each trimeric species expressed in the entire HIV-1 sample is listed for H4/H5 expression ratios 1:0, 1:19, and 0:1. Numbers in the 1:19 column reflect binomial probabilities that assume random assortment of individual protomers into the designated trimer. *B*, relative infectivities of the 1:0, 1:19, and 0:1 HIV-1 samples applied to U87.CD4.CXCR4 target cells. Viral input was normalized to p24 content of each sample. The dotted lines in the 1:19 viral data reflect the relative fractions of the trimeric species plotted on the same relative infectivity scale (blue, (H5)₃; green, (H5)₂(H4); cyan, (H5)(H4)₂; and black, (H4)₃). The red line in the 0:1 viral data reflects the detection limit for viral infection in this set of experiments. The Western blots show the total expression of gp160 (*) and gp41 (**) in HIV-1-producing cells expressing H4/H5 at the ratios indicated on the axis of the plot above. The numbers to the left reflect molecular mass standards in kDa. *C* and *D*, titrations of AMD3100 (*C*) and C37 (*D*) against the 1:0 (black) and 1:19 (red) viral samples. The AMD3100 IC₅₀ values were 26 ± 4.1 and 7.1 ± 0.77 nM, respectively. The C37 IC₅₀ values were 2.8 ± 0.27 and 0.70 ± 0.16 nM, respectively. *E* and *F*, IC₅₀ values for C37 (*E*) and 5H_{WT} (*F*) as a function of AMD3100 concentration for the two HIV-1 samples.

multiple coreceptor binding events that exceeded the number required for viral entry.

Discussion

Synergistic drug combinations provide opportunities for therapeutic augmentation without requiring dose escalations that increase both cost and potential toxicity risks. Synergistic activity arises from drug interactions that can occur at microscopic to macroscopic scales, ranging from a single macromol-

Complex synergy mechanisms of HIV-1 entry inhibitors

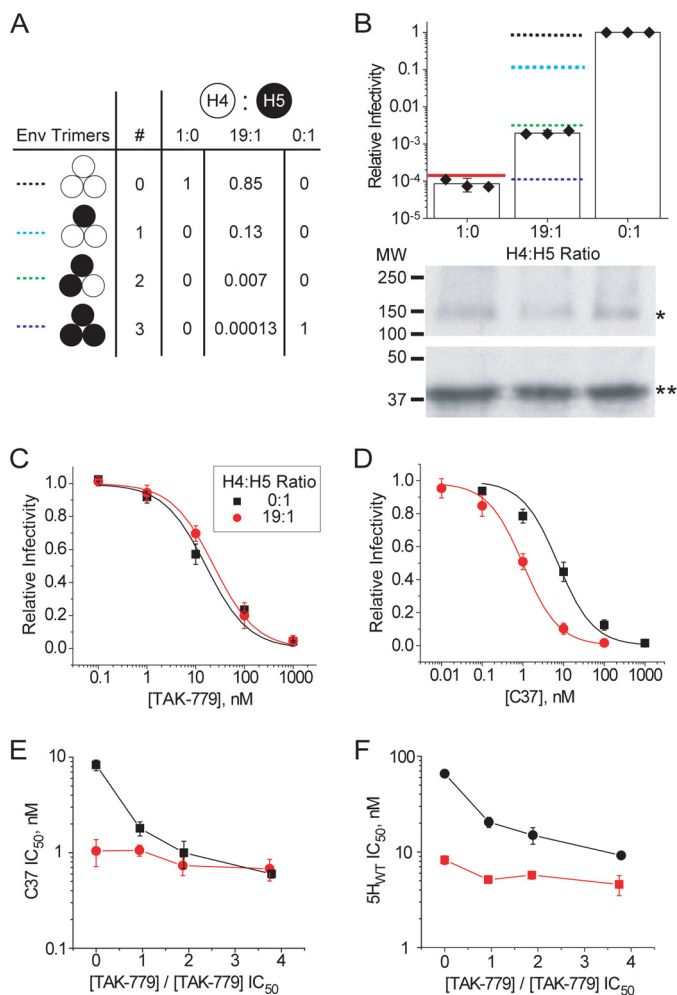


Figure 8. Impact of modifying the number of CCR5-binding sites per Env_{H5} trimer on CoRA/FI synergy. Data are presented as in Fig. 7 except that the experiments utilized U87.CD4.CCR5 cells, TAK-779 as the CoRA, and an H4/H5 expression ratio of 19:1 for the viral sample with mixed Env trimers. *A*, the number of CCR5-binding sites (*column #*) and relative population of each trimer species. *B*, infectivities of the 1:0, 19:1, and 0:1 HIV-1 samples and Env expression levels in virus-producing cells. *C* and *D*, titrations of TAK-779 (*C*) and C37 (*D*) against the 1:0 (*black*) and 19:1 (*red*) viral samples. TAK-779 IC₅₀ values were 17 ± 4.5 and 27 ± 6.2 nM, respectively. C37 IC₅₀ values in the absence of CoRA were 7.9 ± 2.6 and 1.0 ± 0.32 nM, respectively. *E* and *F*, IC₅₀ values for C37 (*E*) and 5H_{WT} (*F*) as a function of TAK779 concentration for the two HIV-1 samples.

ecule (*e.g.* cooperative binding through allostery), to the cell or tissue level (*e.g.* coordinated disruption of multi-protein signaling pathway), and to the whole organism (*e.g.* enhanced bio-availability of an active drug due to reduced *in vivo* clearance caused by a second drug) (59). Mechanistic studies of drug combinations can provide detailed insights into complex multistep biochemical processes. Here, we dissected the complicated synergy profile of two classes of HIV-1 entry inhibitors, CoRAs that block gp120–chemokine receptor interactions and FIs that disrupt conformational transitions in gp41. The data supported the proposed model that synergy for these inhibitors reflects kinetic properties of Env conformational changes. However, our results showed an unanticipated dependence of synergy on coreceptor-binding stoichiometry and FI-binding affinity.

In previous drug combination studies employing molecules that disrupt gp120–coreceptor interactions and C-peptide

T20, synergy was not consistently observed (31, 43–47). Our findings pointed to several possible explanations for this variability. First, we showed that CoRA/FI synergy critically depended on levels of chemokine receptors on target cells, and below some threshold, CoRAs and FIs interacted additively. Discrepancies in chemokine receptor level among different cell lines or among PBMC donors could account for the variance between studies. Second, we demonstrated that the magnitude of synergy between CoRAs and C-peptides like T20 depended on C-peptide-binding affinity, with maximal synergy observed for very high-affinity C-peptide variants, whereas mere additivity was measured for low-affinity C-peptide variants. With T20 having only a modest affinity for gp41 (52), discrepancies in the N-HR sequences of Envs used in different studies could be a source of variability. Finally, we determined that the number of coreceptor binding events required for CoRA/FI synergy exceeded the number required for HIV-1 entry. As differences in gp120–chemokine receptor affinity could alter the coreceptor stoichiometry required for entry, we hypothesize that gp120 sequence variation among Envs used in these studies could impact the level of observed synergy. Further work will be needed to test this conjecture, but the mechanism might be particularly relevant for understanding the wide variety of synergy profiles for clinical HIV-1 isolates in the aforementioned SCH-C/T20 combination study (47).

Our results showed that the level of C37 resistance conferred by the V549E substitution depended on CoRA concentration. The V549E mutation reduced C37 potency 100-fold in the absence of CoRA and 750-fold in the presence of 100 nM AMD3100 (Fig. 2*D*). The result was surprising because the escape mutation influenced FI interaction independently of coreceptor binding. The impact of CoRAs on C37 resistance was traced to disparities in the biophysical determinants of potency for high- and low-affinity FIs (as distinguished by their rates of dissociation relative to the rate of gp41 deactivation). Although the IC₅₀ values for high-affinity (slowly dissociating) FIs depended upon the $I \rightarrow F$ transition rate (k_f , see Fig. 3*C*), IC₅₀ values of low-affinity (rapidly dissociating) FIs depended upon the ratio of the $I \rightarrow F$ and $IX \rightarrow D$ transition rates (k_f/k_s). FI potency was enhanced by a CoRA-dependent decrease in k_f . However, that effect was mitigated for low-affinity C37 variants because both k_f and k_s have the same dependence on target-cell coreceptor levels for inhibitors targeting the gp41 N-HR. This switch in determinants for C37 potency accounted for the loss of CoRA/FI synergy in the setting of affinity-disrupting escape mutations. This loss nullifies a potentially important benefit of synergistic antiviral combinations, specifically the possibility that inhibitor concentrations might be maintained in a useful therapeutic window even when resistance mutations would render one inhibitor poorly efficacious in the absence of a synergistic partner. Curiously, CoRA/FI synergy persisted for low-affinity 5-Helix variants. The results reinforced the idea that N-HR-targeted and C-HR-targeted FIs trigger irreversible gp41 deactivation ($IX \rightarrow D$ transition) through very different mechanisms (38).

In addition to gp120–coreceptor interactions, substitutions in the gp41 N-HR and C-HR regions can influence the lifetime of the PHI (54, 55). How such mutations impact the fusion

rate is not known. Given the packing of gp120 around gp41 in the native state (and possibly the PHI (58)), it is formally possible that gp41 substitutions could exert effects on gp120 structure and indirectly alter coreceptor utilization by Env. In this study, the k_f -altering substitutions L565Q and N637K/T639I did not have a large impact on CoRA potency. Furthermore, both the slower and faster Env variants showed the same synergy profile (both in magnitude and concentration dependence) as wild-type Env. Together, the data suggested that these gp41 substitutions exerted minimal impact on coreceptor utilization by Env. Instead, the results implied that the gp41 sequence sets a basal lifetime for the PHI (observed at high CoRA concentrations) that can be shortened by excess coreceptor binding.

Our findings also offered insights into the timing of coreceptor binding events coordinating Env conformational changes. In one model of HIV-1 entry, CD4 binding to the native state drives Env into the PHI, whereas coreceptor binding during the PHI triggers collapse into the TOH (60). This model explained how coreceptor levels on target cells influence PHI lifetime and FI potency. In support of this model, soluble CD4 (sCD4) alone was shown to be sufficient to trigger Env to expose FI-binding sites in gp41 pulldown and Env-mediated membrane fusion assays (of note, these studies employed laboratory-adapted Env strains prone to rapid and efficient sCD4-induced gp120 shedding) (17, 18, 20, 61, 62). However, the model failed to explain the difference between CoRAs and FIs observed in time-of-addition assays (37, 39). In these studies, escape from CoRA inhibition occurred considerably before escape from FI inhibition, implying that coreceptor binding significantly preceded collapse into the TOH. Our results showing an absence of CoRA/FI synergy at low coreceptor-binding stoichiometry suggested a solution to this inconsistency; the first coreceptor-binding event precedes and facilitates transformation into the PHI, whereas subsequent coreceptor binding events during the PHI promote collapse into the TOH. Only the first coreceptor binding event is absolutely required for HIV-1 entry, whereas subsequent binding events primarily modulate the rate of fusion. Env species mediating fusion meet only the minimal coreceptor-binding requirement when coreceptor levels on target cells are low or Env trimers contain one functional coreceptor-binding site. Because Env does not interact with additional coreceptors, the PHI lifetime remains unmodulated, and FI potency becomes CoRA independent.

Based on the functionality of H4/H5 mixtures, our model currently assumes that a single coreceptor binding event is sufficient to drive transformation into the PHI. However, the model would remain valid if two coreceptor binding events were required to facilitate this transition, and only the third modulated the PHI lifetime. Indeed, results from this study suggest that different Env strains may have different coreceptor-binding requirements for entry (e.g. compare the fusogenic activities of HIV-1 pseudotyped with H4/H5 mixtures in Figs. 7B and 8B). Future work with better defined Env heterotrimers will be needed to piece together the exact stoichiometries of coreceptor binding that facilitate the transition of Env into the PHI and, ultimately, the TOH.

Experimental procedures

Cell lines and reagents

The following cell lines and reagents were obtained through the AIDS Research and Reference Reagent Program, Division of AIDS, NIAID, National Institutes of Health: U87.CD4.CXCR4 and U87.CD4.CCR5 cells from Drs. HongKui Deng and Dan Littman (63); Chessie 8 hybridoma from Dr. George Lewis (64); maraviroc (11580) (65, 66); AMD-3100 (67, 68); and TAK779 (69). HEK 293T cells were obtained from the ATCC. JC.53 and JC.10 cells were kindly provided by Dr. David Kabat (Oregon Health Sciences University) (57). PIE12 fusion inhibitors were kindly provided by Dr. Michael Kay (University of Utah) (56).

Fusion inhibitor preparation

C-peptide T20 was synthesized using standard Fmoc (*N*-(9-fluorenyl)methoxycarbonyl) chemistry by the Peptide Synthesis Facility at the Sidney Kimmel Cancer Center, Thomas Jefferson University. Cleaved, desalted peptides were purified to homogeneity by reverse phase-HPLC using a Vydac C18 column and a linear gradient of acetonitrile in water containing 0.1% trifluoroacetic acid. C-peptide C37 and its variants were prepared from a recombinant gp41 TOH construct NC1 as described previously (28, 38). Briefly, NC1 was recombinantly expressed and purified from bacterial lysates by metal-chelate chromatography and subsequently subjected to trypsin digestion to cleave C37 from the N-HR peptide N40. C37 was purified to homogeneity using reverse phase-HPLC as described above. Di-C37 is a dimerized form of C37 connected via an engineered disulfide bond at the C terminus of each monomer (38).

5-Helix proteins contain three N40 segments and two C37 segments alternately connected by short linkers into a single polypeptide (28). The proteins were recombinantly expressed and purified as described previously (19). Briefly, 5-Helix was solubilized from bacterial inclusion bodies using 8 M guanidine HCl in Tris-buffered saline (TBS), loaded onto nickel-nitrilotriacetic acid-agarose beads (Qiagen), and renatured in 4 M guanidine HCl by a reverse thermal gradient (90 °C to room temperature over 4 h). Aggregates were separated from properly folded protein by size-exclusion chromatography (Superdex 75, GE Healthcare).

The concentrations of T20, PIE12 trimer, C37 peptides, and 5-Helix proteins were determined by absorbance at 280 nm by the method of Edelhoch (70). The interaction and inhibition properties of these inhibitors have been extensively characterized (19, 38, 52, 56).

HIV-1 production and characterization

HIV-1 particles were prepared from 293T cells (5×10^6) transfected (X-tremeGENE, Roche Applied Science) with 2.5 μ g of Env-deficient HIV-1_{NL4-3} genome pNL4-3R⁻E⁻Luc⁺ (71) and 2.5 μ g (total) of one or two Env-expressing plasmids (pEBB_Env_X, X = HXB2, JR-FL, BaL, and H5). Env_{H5} is an Env_{HXB2} variant with a V3 loop derived from CCR5-tropic Env_{SF162} (58). Virus-containing supernatants were harvested 48 h post-transfection and were used fresh for infectivity studies described below. Virus-producing cells were lysed and ana-

Complex synergy mechanisms of HIV-1 entry inhibitors

lyzed by Western blotting for expression of Env. Briefly, lysates were clarified by centrifugation, and the protein contents of the supernatants were determined by Bradford analysis (Thermo Fisher Scientific). Lysate aliquots normalized by protein content were separated by SDS-PAGE (10%), transferred to nitrocellulose paper (GE Healthcare), and probed with monoclonal antibody Chessie 8, which recognizes an epitope in the gp160 and gp41 cytoplasmic tail (64). Western blottings were developed with an HRP-conjugated secondary antibody (Jackson ImmunoResearch) and ECL reagent kit (Pierce).

HIV-1 infection was measured on U87 cells, except as noted in Fig. 6. Cells were plated at a density of 20,000 per well in 48-well plates 18–24 h prior to infection. On the day of infection, media were replaced with HIV-1-containing supernatant (see above) and fresh media containing one or two inhibitors as indicated. After 36–48 h, the cells were lysed in 1% Triton X-100, and levels of the luciferase reporter were assessed by luminescence (Promega or Pierce). To measure fusogenic activities of HIV-1 particles pseudotyped with Env strain H4, H5, or a mixture of H4 and H5 (Figs. 7B and 8B), luciferase activity was normalized to p24 content of the viral sample determined by ELISA (Aalto, Ireland).

Inhibitor titrations of viral infection were fit to the simple dose-response Langmuir equation (Equation 1) to extract IC_{50} values. This choice was supported by the observation that the vast majority of titrations (>97%) fit to the Hill equation with a Hill coefficient n_H between 0.9 and 1.1.

Author contributions—K. W. A. and M. J. R. conceived the idea for the project. K. W. A. conducted the experiments and analyzed the data. K. W. A. and M. J. R. interpreted the results and wrote the manuscript.

Acknowledgments—We thank Dr. D. Kabat for cell lines JC.10 and JC.53; Dr. M. Kay for D-peptide PIE12 trimer; Drs. M. Khasnis and K. Halkidis for helpful discussions; Drs. J. Benovic, P. Wedegaertner, C. Scott, and members of the Root laboratory for critical evaluation of the manuscript. Research in this publication includes work carried out at the Sidney Kimmel Cancer Center X-ray Crystallography and Molecular Characterization Shared Resource at Thomas Jefferson University, which is supported in part by National Institutes of Health NCI Cancer Center Support Grant P30 CA056036.

Note added in proof—In the version of this article that was published as a Paper in Press on July 10, 2017, the titration curve from 19:1 viral samples in Fig. 8D inadvertently duplicated the titration curve from 1:19 viral samples from Fig. 7D. This error has now been corrected and does not affect the results or conclusions of this work.

References

1. Checkley, M. A., Lutge, B. G., and Freed, E. O. (2011) HIV-1 envelope glycoprotein biosynthesis, trafficking, and incorporation. *J. Mol. Biol.* **410**, 582–608
2. Zanetti, G., Briggs, J. A., Grünewald, K., Sattentau, Q. J., and Fuller, S. D. (2006) Cryo-electron tomographic structure of an immunodeficiency virus envelope complex *in situ*. *PLoS Pathog.* **2**, e83
3. Liu, J., Bartesaghi, A., Borgnia, M. J., Sapiro, G., and Subramaniam, S. (2008) Molecular architecture of native HIV-1 gp120 trimers. *Nature* **455**, 109–113
4. White, T. A., Bartesaghi, A., Borgnia, M. J., Meyerson, J. R., de la Cruz, M. J., Bess, J. W., Nandwani, R., Hoxie, J. A., Lifson, J. D., Milne, J. L., and Subramaniam, S. (2010) Molecular architectures of trimeric SIV and HIV-1 envelope glycoproteins on intact viruses: strain-dependent variation in quaternary structure. *PLoS Pathog.* **6**, e1001249
5. Julien, J. P., Cupo, A., Sok, D., Stanfield, R. L., Lyumkis, D., Deller, M. C., Klasse, P. J., Burton, D. R., Sanders, R. W., Moore, J. P., Ward, A. B., and Wilson, I. A. (2013) Crystal structure of a soluble cleaved HIV-1 envelope trimer. *Science* **342**, 1477–1483
6. Lyumkis, D., Julien, J. P., de Val, N., Cupo, A., Potter, C. S., Klasse, P. J., Burton, D. R., Sanders, R. W., Moore, J. P., Carragher, B., Wilson, I. A., and Ward, A. B. (2013) Cryo-EM structure of a fully glycosylated soluble cleaved HIV-1 envelope trimer. *Science* **342**, 1484–1490
7. Pancera, M., Zhou, T., Druz, A., Georgiev, I. S., Soto, C., Gorman, J., Huang, J., Acharya, P., Chuang, G. Y., Ofek, G., Stewart-Jones, G. B., Stuckey, J., Bailer, R. T., Joyce, M. G., Louder, M. K., et al. (2014) Structure and immune recognition of trimeric pre-fusion HIV-1 Env. *Nature* **514**, 455–461
8. Eckert, D. M., and Kim, P. S. (2001) Mechanisms of viral membrane fusion and its inhibition. *Annu. Rev. Biochem.* **70**, 777–810
9. Harrison, S. C. (2008) Viral membrane fusion. *Nat. Struct. Mol. Biol.* **15**, 690–698
10. Melikyan, G. B. (2011) Membrane fusion mediated by human immunodeficiency virus envelope glycoprotein. *Curr. Top. Membr.* **68**, 81–106
11. Kwong, P. D., Wyatt, R., Robinson, J., Sweet, R. W., Sodroski, J., and Hendrickson, W. A. (1998) Structure of an HIV gp120 envelope glycoprotein in complex with the CD4 receptor and a neutralizing human antibody. *Nature* **393**, 648–659
12. Berger, E. A., Murphy, P. M., and Farber, J. M. (1999) Chemokine receptors as HIV-1 coreceptors: roles in viral entry, tropism, and disease. *Annu. Rev. Immunol.* **17**, 657–700
13. Melikyan, G. B., Platt, E. J., and Kabat, D. (2007) The role of the N-terminal segment of CCR5 in HIV-1 Env-mediated membrane fusion and the mechanism of virus adaptation to CCR5 lacking this segment. *Retrovirology* **4**, 55
14. Platt, E. J., Shea, D. M., Rose, P. P., and Kabat, D. (2005) Variants of human immunodeficiency virus-type 1 that efficiently use CCR5 lacking the tyrosine-sulfated amino terminus have adaptive mutations in gp120, including loss of a functional N-glycan. *J. Virol.* **79**, 4357–4368
15. Wu, L., Gerard, N. P., Wyatt, R., Choe, H., Parolin, C., Ruffing, N., Borsetti, A., Cardoso, A. A., Desjardins, E., Newman, W., Gerard, C., and Sodroski, J. (1996) CD4-induced interaction of primary HIV-1 gp120 glycoproteins with the chemokine receptor CCR-5. *Nature* **384**, 179–183
16. Muñoz-Barroso, I., Durell, S., Sakaguchi, K., Appella, E., and Blumenthal, R. (1998) Dilatation of the human immunodeficiency virus-1 envelope glycoprotein fusion pore revealed by the inhibitory action of a synthetic peptide from gp41. *J. Cell Biol.* **140**, 315–323
17. Furuta, R. A., Wild, C. T., Weng, Y., and Weiss, C. D. (1998) Capture of an early fusion-active conformation of HIV-1 gp41. *Nat. Struct. Biol.* **5**, 276–279
18. Melikyan, G. B., Markosyan, R. M., Hemmati, H., Delmedico, M. K., Lambert, D. M., and Cohen, F. S. (2000) Evidence that the transition of HIV-1 gp41 into a six-helix bundle, not the bundle configuration, induces membrane fusion. *J. Cell Biol.* **151**, 413–423
19. Steger, H. K., and Root, M. J. (2006) Kinetic dependence to HIV-1 entry inhibition. *J. Biol. Chem.* **281**, 25813–25821
20. Kilgore, N. R., Salzwedel, K., Reddick, M., Allaway, G. P., and Wild, C. T. (2003) Direct evidence that C-peptide inhibitors of human immunodeficiency virus-type 1 entry bind to the gp41 N-helical domain in receptor-activated viral envelope. *J. Virol.* **77**, 7669–7672
21. Chan, D. C., Fass, D., Berger, J. M., and Kim, P. S. (1997) Core structure of gp41 from the HIV envelope glycoprotein. *Cell* **89**, 263–273
22. Weissenhorn, W., Dessen, A., Harrison, S. C., Skehel, J. J., and Wiley, D. C. (1997) Atomic structure of the ectodomain from HIV-1 gp41. *Nature* **387**, 426–430
23. Lederman, M. M., Jump, R., Pilch-Cooper, H. A., Root, M., and Sieg, S. F. (2008) Topical application of entry inhibitors as “virustats” to prevent sexual transmission of HIV infection. *Retrovirology* **5**, 116
24. Shaheen, F., and Collman, R. G. (2004) Co-receptor antagonists as HIV-1 entry inhibitors. *Curr. Opin. Infect. Dis.* **17**, 7–16

25. Wild, C. T., Shugars, D. C., Greenwell, T. K., McDanal, C. B., and Matthews, T. J. (1994) Peptides corresponding to a predictive α -helical domain of human immunodeficiency virus-type 1 gp41 are potent inhibitors of virus infection. *Proc. Natl. Acad. Sci. U.S.A.* **91**, 9770–9774
26. Jiang, S., Lin, K., Strick, N., and Neurath, A. R. (1993) HIV-1 inhibition by a peptide. *Nature* **365**, 113
27. Lu, M., Blacklow, S. C., and Kim, P. S. (1995) A trimeric structural domain of the HIV-1 transmembrane glycoprotein. *Nat. Struct. Biol.* **2**, 1075–1082
28. Root, M. J., Kay, M. S., and Kim, P. S. (2001) Protein design of an HIV-1 entry inhibitor. *Science* **291**, 884–888
29. Eckert, D. M., and Kim, P. S. (2001) Design of potent inhibitors of HIV-1 entry from the gp41 N-peptide region. *Proc. Natl. Acad. Sci. U.S.A.* **98**, 11187–11192
30. Louis, J. M., Bewley, C. A., and Clore, G. M. (2001) Design and properties of N(CCG)-gp41, a chimeric gp41 molecule with nanomolar HIV fusion inhibitory activity. *J. Biol. Chem.* **276**, 29485–29489
31. Dorr, P., Westby, M., Dobbs, S., Griffin, P., Irvine, B., Macartney, M., Mori, J., Rickett, G., Smith-Burchnell, C., Napier, C., Webster, R., Armour, D., Price, D., Stammen, B., Wood, A., and Perros, M. (2005) Maraviroc (UK-427,857), a potent, orally bioavailable, and selective small-molecule inhibitor of chemokine receptor CCR5 with broad-spectrum anti-human immunodeficiency virus-type 1 activity. *Antimicrob. Agents Chemother.* **49**, 4721–4732
32. Lieberman-Blum, S. S., Fung, H. B., and Bandres, J. C. (2008) Maraviroc: a CCR5-receptor antagonist for the treatment of HIV-1 infection. *Clin. Ther.* **30**, 1228–1250
33. Berkhout, B., Eggink, D., and Sanders, R. W. (2012) Is there a future for antiviral fusion inhibitors? *Curr. Opin. Virol.* **2**, 50–59
34. Gupta, R. K., Loveday, C., Kalidindi, U., Lechelt, M., Skinner, C., and Orkin, C. (2007) Tipranavir/T20-based salvage regimens highly effective and durable against HIV-1 with evidence for genotypic predictability of response in clinical practice. *Int. J. STD AIDS* **18**, 630–632
35. Reeves, J. D., Gallo, S. A., Ahmad, N., Miamidian, J. L., Harvey, P. E., Sharron, M., Pohlmann, S., Sfakianos, J. N., Derdeyn, C. A., Blumenthal, R., Hunter, E., and Doms, R. W. (2002) Sensitivity of HIV-1 to entry inhibitors correlates with envelope/coreceptor affinity, receptor density, and fusion kinetics. *Proc. Natl. Acad. Sci. U.S.A.* **99**, 16249–16254
36. Abrahamyan, L. G., Mkrtchyan, S. R., Binley, J., Lu, M., Melikyan, G. B., and Cohen, F. S. (2005) The cytoplasmic tail slows the folding of human immunodeficiency virus-type 1 Env from a late prebundle configuration into the six-helix bundle. *J. Virol.* **79**, 106–115
37. Miyauchi, K., Kozlov, M. M., and Melikyan, G. B. (2009) Early steps of HIV-1 fusion define the sensitivity to inhibitory peptides that block 6-helix bundle formation. *PLoS Pathog.* **5**, e1000585
38. Kahle, K. M., Steger, H. K., and Root, M. J. (2009) Asymmetric deactivation of HIV-1 gp41 following fusion inhibitor binding. *PLoS Pathog.* **5**, e1000674
39. Platt, E. J., Durnin, J. P., and Kabat, D. (2005) Kinetic factors control efficiencies of cell entry, efficacies of entry inhibitors, and mechanisms of adaptation of human immunodeficiency virus. *J. Virol.* **79**, 4347–4356
40. Reeves, J. D., Miamidian, J. L., Biscone, M. J., Lee, F. H., Ahmad, N., Pierson, T. C., and Doms, R. W. (2004) Impact of mutations in the coreceptor binding site on human immunodeficiency virus-type 1 fusion, infection, and entry inhibitor sensitivity. *J. Virol.* **78**, 5476–5485
41. Heredia, A., Gilliam, B., DeVico, A., Le, N., Bamba, D., Flinko, R., Lewis, G., Gallo, R. C., and Redfield, R. R. (2007) CCR5 density levels on primary CD4 T cells impact the replication and Enfuvirtide susceptibility of R5 HIV-1. *AIDS* **21**, 1317–1322
42. Heredia, A., Gilliam, B., Latinovic, O., Le, N., Bamba, D., DeVico, A., Melikyan, G. B., Gallo, R. C., and Redfield, R. R. (2007) Rapamycin reduces CCR5 density levels on CD4 T cells, and this effect results in potentiation of enfuvirtide (T-20) against R5 strains of human immunodeficiency virus-type 1 *in vitro*. *Antimicrob. Agents Chemother.* **51**, 2489–2496
43. Tremblay, C. L., Kollmann, C., Giguel, F., Chou, T. C., and Hirsch, M. S. (2000) Strong *in vitro* synergy between the fusion inhibitor T-20 and the CXCR4 blocker AMD-3100. *J. Acquir. Immune Defic. Syndr.* **25**, 99–102
44. Ji, C., Zhang, J., Dioszegi, M., Chiu, S., Rao, E., Derosier, A., Cammack, N., Brandt, M., and Sankuratri, S. (2007) CCR5 small-molecule antagonists and monoclonal antibodies exert potent synergistic antiviral effects by cobinding to the receptor. *Mol. Pharmacol.* **72**, 18–28
45. Ketas, T. J., Holuigue, S., Matthews, K., Moore, J. P., and Klasse, P. J. (2012) Env-glycoprotein heterogeneity as a source of apparent synergy and enhanced cooperativity in inhibition of HIV-1 infection by neutralizing antibodies and entry inhibitors. *Virology* **422**, 22–36
46. Murga, J. D., Franti, M., Pevear, D. C., Maddon, P. J., and Olson, W. C. (2006) Potent antiviral synergy between monoclonal antibody and small-molecule CCR5 inhibitors of human immunodeficiency virus-type 1. *Antimicrob. Agents Chemother.* **50**, 3289–3296
47. Tremblay, C. L., Giguel, F., Kollmann, C., Guan, Y., Chou, T. C., Baroudy, B. M., and Hirsch, M. S. (2002) Anti-human immunodeficiency virus interactions of SCH-C (SCH 351125), a CCR5 antagonist, with other anti-retroviral agents *in vitro*. *Antimicrob. Agents Chemother.* **46**, 1336–1339
48. Chou, T. C., and Talalay, P. (1984) Quantitative analysis of dose-effect relationships: the combined effects of multiple drugs or enzyme inhibitors. *Adv. Enzyme Regul.* **22**, 27–55
49. Chou, T. C. (2006) Theoretical basis, experimental design, and computerized simulation of synergism and antagonism in drug combination studies. *Pharmacol. Rev.* **58**, 621–681
50. Breiting, H.-G. (2012) in *Toxicity and Drug Testing* (Acree, B. ed.) Int-Tech, 10.5772/30922
51. Rimsky, L. T., Shugars, D. C., and Matthews, T. J. (1998) Determinants of human immunodeficiency virus-type 1 resistance to gp41-derived inhibitory peptides. *J. Virol.* **72**, 986–993
52. Champagne, K., Shishido, A., and Root, M. J. (2009) Interactions of HIV-1 inhibitory peptide T20 with the gp41 N-HR coiled coil. *J. Biol. Chem.* **284**, 3619–3627
53. Armand-Ugón, M., Gutiérrez, A., Clotet, B., and Esté, J. A. (2003) HIV-1 resistance to the gp41-dependent fusion inhibitor C-34. *Antiviral Res.* **59**, 137–142
54. Ray, N., Harrison, J. E., Blackburn, L. A., Martin, J. N., Deeks, S. G., and Doms, R. W. (2007) Clinical resistance to enfuvirtide does not affect susceptibility of human immunodeficiency virus-type 1 to other classes of entry inhibitors. *J. Virol.* **81**, 3240–3250
55. Reeves, J. D., Lee, F. H., Miamidian, J. L., Jabara, C. B., Juntilla, M. M., and Doms, R. W. (2005) Enfuvirtide resistance mutations: impact on human immunodeficiency virus envelope function, entry inhibitor sensitivity, and virus neutralization. *J. Virol.* **79**, 4991–4999
56. Welch, B. D., Francis, J. N., Redman, J. S., Paul, S., Weinstock, M. T., Reeves, J. D., Lie, Y. S., Whitby, F. G., Eckert, D. M., Hill, C. P., Root, M. J., and Kay, M. S. (2010) Design of a potent D-peptide HIV-1 entry inhibitor with a strong barrier to resistance. *J. Virol.* **84**, 11235–11244
57. Platt, E. J., Wehrly, K., Kuhmann, S. E., Chesebro, B., and Kabat, D. (1998) Effects of CCR5 and CD4 cell surface concentrations on infections by macrophagetropic isolates of human immunodeficiency virus-type 1. *J. Virol.* **72**, 2855–2864
58. Khasnis, M. D., Halkidis, K., Bhardwaj, A., and Root, M. J. (2016) Receptor activation of HIV-1 Env leads to asymmetric exposure of the gp41 trimer. *PLoS Pathog.* **12**, e1006098
59. Jia, J., Zhu, F., Ma, X., Cao, Z., Cao, Z. W., Li, Y., Li, Y. X., and Chen, Y. Z. (2009) Mechanisms of drug combinations: interaction and network perspectives. *Nat. Rev. Drug Discov.* **8**, 111–128
60. Root, M. J., and Steger, H. K. (2004) HIV-1 gp41 as a target for viral entry inhibition. *Curr. Pharm. Des.* **10**, 1805–1825
61. Koshiba, T., and Chan, D. C. (2003) The prefusogenic intermediate of HIV-1 gp41 contains exposed C-peptide regions. *J. Biol. Chem.* **278**, 7573–7579
62. Root, M. J., and Hamer, D. H. (2003) Targeting therapeutics to an exposed and conserved binding element of the HIV-1 fusion protein. *Proc. Natl. Acad. Sci. U.S.A.* **100**, 5016–5021
63. Björndal, A., Deng, H., Jansson, M., Fiore, J. R., Colognesi, C., Karlsson, A., Albert, J., Scarlatti, G., Littman, D. R., and Fenyö, E. M. (1997) Coreceptor usage of primary human immunodeficiency virus-type 1 isolates varies according to biological phenotype. *J. Virol.* **71**, 7478–7487
64. Abacioglu, Y. H., Fouts, T. R., Laman, J. D., Claassen, E., Pincus, S. H., Moore, J. P., Roby, C. A., Kamin-Lewis, R., and Lewis, G. K. (1994) Epitope

Complex synergy mechanisms of HIV-1 entry inhibitors

- mapping and topology of baculovirus-expressed HIV-1 gp160 determined with a panel of murine monoclonal antibodies. *AIDS Res. Hum. Retroviruses* **10**, 371–381
65. Emmelkamp, J. M., and Rockstroh, J. K. (2007) CCR5 antagonists: comparison of efficacy, side effects, pharmacokinetics and interactions—review of the literature. *Eur. J. Med. Res.* **12**, 409–417
66. Biswas, P., Tambussi, G., and Lazzarin, A. (2007) Access denied? The status of co-receptor inhibition to counter HIV entry. *Expert Opin. Pharmacother.* **8**, 923–933
67. De Clercq, E., Yamamoto, N., Pauwels, R., Balzarini, J., Witvrouw, M., De Vreese, K., Debyser, Z., Rosenwirth, B., Peichl, P., and Datema, R. (1994) Highly potent and selective inhibition of human immunodeficiency virus by the bicyclam derivative JM3100. *Antimicrob. Agents Chemother.* **38**, 668–674
68. Bridger, G. J., Skerlj, R. T., Thornton, D., Padmanabhan, S., Martellucci, S. A., Henson, G. W., Abrams, M. J., Yamamoto, N., De Vreese, K., and Pauwels, R. (1995) Synthesis and structure-activity relationships of phenylenebis(methylene)-linked bis-tetraazamacrocycles that inhibit HIV replication. Effects of macrocyclic ring size and substituents on the aromatic linker. *J. Med. Chem.* **38**, 366–378
69. Baba, M., Nishimura, O., Kanzaki, N., Okamoto, M., Sawada, H., Iizawa, Y., Shiraishi, M., Aramaki, Y., Okonogi, K., Ogawa, Y., Meguro, K., and Fujino, M. (1999) A small-molecule, nonpeptide CCR5 antagonist with highly potent and selective anti-HIV-1 activity. *Proc. Natl. Acad. Sci. U.S.A.* **96**, 5698–5703
70. Edelhofer, H. (1967) Spectroscopic determination of tryptophan and tyrosine in proteins. *Biochemistry* **6**, 1948–1954
71. Chen, B. K., Saksela, K., Andino, R., and Baltimore, D. (1994) Distinct modes of human immunodeficiency virus-type 1 proviral latency revealed by superinfection of nonproductively infected cell lines with recombinant luciferase-encoding viruses. *J. Virol.* **68**, 654–660

Complex interplay of kinetic factors governs the synergistic properties of HIV-1 entry inhibitors

Koree W. Ahn and Michael J. Root

J. Biol. Chem. 2017, 292:16498-16510.

doi: 10.1074/jbc.M117.791731 originally published online July 10, 2017

Access the most updated version of this article at doi: [10.1074/jbc.M117.791731](https://doi.org/10.1074/jbc.M117.791731)

Alerts:

- [When this article is cited](#)
- [When a correction for this article is posted](#)

[Click here](#) to choose from all of JBC's e-mail alerts

This article cites 70 references, 33 of which can be accessed free at <http://www.jbc.org/content/292/40/16498.full.html#ref-list-1>